

PFlow-T: A Persistence-Driven Forward Process for Topology-Controlled Generation

Snigdha Chandan Khilar

Independent Researcher
snkhilar@gmail.com

Abstract

Current topology-aware diffusion models suffer from a fundamental architectural mismatch: they corrupt inputs with topology-agnostic Gaussian noise but attempt to recover structural features via conditional side channels in the reverse network. To resolve this, the authors introduce PFlow-T, a novel generative model that defines its forward diffusion process entirely through the persistent homology of the data.

In PFlow-T, the time parameter does not track Gaussian noise injection; instead, it measures the fraction of H_1 persistence-mass that has been destroyed. The forward operator systematically eliminates H_1 topological features (such as holes) in strict ascending order of their persistence. Because the corruption is topologically structured, the reverse network learns to directly invert it to predict the clean state (x_0) in a single inference step, rather than retrieving topology from external conditioning.

Empirical evaluations on MNIST digits ($\{0, 1, 8\}$) demonstrate that PFlow-T drastically outperforms a parameter-matched DDPM baseline conditioned on a 64-d persistence landscape. PFlow-T successfully honors the requested Betti numbers ($\beta_1 \in \{0, 1, 2\}$) in 99.6%, 96.0%, and 84.8% of generations, compared to the baseline’s 96.4%, 3.2%, and 0.0% (an average gap of 88.8 percentage points for $\beta_1 \geq 1$). Furthermore, on out-of-distribution conditioning tasks—where the model must generate a topology contradicting the digit’s class prior—PFlow-T succeeds in 92.0% of cases versus the baseline’s 9.7%.

PFlow-T stands as the first generative architecture where persistent homology acts as the core substrate of the forward process. The authors acknowledge current scope limitations, noting that the forward operator is a pixel-space proxy for exact Edelsbrunner–Harer pair cancellation and is tested at low resolutions, leaving a faithful persistence-module state space for future work.

1 Introduction

A surprising fraction of the data we want generative models to produce has topology in it. Molecules have rings. Vascular networks have loops. Floor plans have enclosed rooms. Digits have holes (the 0 has one, the 8 has two, the 1 has none). For all of these, “getting the picture roughly right” is not enough; what matters is whether the right number of loops, voids, or components show up in the output.

The standard recipe in the diffusion literature is to corrupt the data with Gaussian noise, then ask the reverse network to reconstruct it while conditioning on some topological descriptor of the target. This is the approach taken by Hu et al. [9] on 3D shapes, TAGG [14] on molecular graphs, TopoDiffusionNet [7] on 2D binary masks, and the recent ZS-DM [4] that uses zigzag persistence descriptors as conditioning. The common thread is that the forward process itself has nothing to do

with topology; topology is a side channel that flows into the denoiser through cross-attention or as an embedding.

There is something architecturally awkward about this. The forward process destroys topology indiscriminately, and we then ask a finite-capacity network to recover that topology from a description of what it should be. The denoiser is fighting its own noise model on every step. The fact that this works at all is a testament to how well overparameterised diffusion models can be, but it leaves a structural question on the table: what would happen if the forward process were *itself* defined in terms of topology? Could a network learn to invert a noise process that already knew about holes?

An intuition for non-experts. A standard diffusion model works by gradually scrambling a clean image into pure random noise (this is the forward process), and then training a neural network to undo that scrambling step by step (the reverse process). To make such a model produce a digit “8” specifically — which has two holes — researchers typically hand the reverse network an extra hint: “please produce something with two holes.” The network now has two jobs at once: it must denoise random pixels back into a coherent image *and* simultaneously honour the topology request. These two jobs pull in different directions, because the noise process doesn’t know or care about holes; the topology requirement is essentially a constraint the network has to satisfy on the side. With enough parameters and training data, models can usually meet both demands at once, but the architecture is fighting itself. PFlow-T removes the conflict by changing what the forward process *does*: instead of scrambling pixels randomly, it fills in the smallest hole first, then the next-smallest, and so on, until at the end all holes are gone. The reverse network’s only job is to “un-fill” the holes in the right order. Topology control is no longer a constraint to satisfy alongside denoising; it *is* the denoising.

This is the question this paper takes seriously. We define a forward operator whose action and whose time parameter are both specified in terms of persistent homology. The state at time t is no longer “the image, but with more noise” but rather “the image, but with the smaller holes filled in.” We train a reverse network to undo this process, and we find that the resulting model honours topology requests with substantially higher fidelity than a parameter-matched conditioning baseline that has access to richer topological information.

We are not claiming this resolves the broader problem of topology-controlled generation. We are claiming something narrower and, we think, useful: that there is a structurally distinct point in the design space that prior work has not occupied, that it can be implemented, and that on the small benchmark we have run it on, it outperforms the alternative by a margin that is hard to dismiss as a coincidence of hyperparameters.

Contributions.

- We define a forward operator whose action and time parameter are derived from persistent homology, and we show its monotonicity in β_1 (Section 4).
- We position PFlow-T outside the GenPhys [11] family of PDE-based generative models: the substrate is a filtered chain complex, not a measure space, and the time parameter is a persistence threshold, not a clock (Section 5).
- On a small but careful MNIST controllability benchmark we report an 88.8pp gap on $\beta_1 \geq 1$ classes over a parameter-matched DDPM conditioned on a 64-d persistence landscape, and an 82.3pp gap on out-of-distribution conditioning (Section 6).
- We are explicit about what is and is not done. The forward operator is a pixel-space proxy for

true pair cancellation; the state is the image, not the persistence module; the experiments are on three MNIST classes (Section 7).

Code. A reference implementation, with scripts that reproduce every numerical result and figure in the paper, is available at <https://github.com/nssprogrammer/pflow>. The repository includes the persistence-melt forward operator, the x_0 -prediction reverse network, the persistence-landscape baseline, and the multi-seed evaluation runners.

2 A short tour of persistent homology

This section is for readers who have not seen persistent homology before. Readers who have can skip to Section 3.

Topology, very informally, is the study of shape properties that survive continuous deformation. A coffee cup and a donut are topologically the same shape because each has one hole; squishing the cup smoothly into the donut never destroys or creates a hole. What is invariant under this kind of deformation is captured by the *Betti numbers*: β_0 counts the number of connected components, β_1 counts the number of one-dimensional holes (loops), β_2 counts the number of two-dimensional voids (cavities), and so on. For the MNIST examples that motivate this paper, the relevant invariant is β_1 : the digit 1 has $\beta_1 = 0$ (no loops), the digit 0 has $\beta_1 = 1$ (the enclosed interior of the loop), and the digit 8 has $\beta_1 = 2$.

Real images do not arrive as the abstract topological spaces that Betti numbers were originally defined on. They arrive as arrays of pixel intensities, and the topology depends on where you decide to draw the line between “foreground” and “background.” If the threshold is set too low, the digit’s strokes merge into a single blob; too high, and they disintegrate into isolated dots. Persistent homology resolves this by refusing to commit to a single threshold: it sweeps a threshold parameter from 0 to 1 (or any other range) and records every topological feature as a pair (b, d) , where b is the threshold at which the feature first appears and d the threshold at which it disappears. The difference $d - b$, called the *persistence*, is how long the feature survives across thresholds.

Persistent features are the ones that genuinely belong to the shape. Short-lived features are usually noise: a one-pixel speckle that appears at some specific threshold and vanishes immediately. Sorting features by persistence and ignoring the short ones is the standard way to extract a robust topological signature from a noisy image.

For our purposes the relevant facts are: (i) we can compute, for any 28×28 MNIST image, a list of H_1 features (loops) together with their birth and death thresholds; (ii) we can sort these by persistence; and (iii) for each feature, we know roughly where in the image the loop sits, because the death of an H_1 feature is recorded at a specific pixel (the saddle that closes the loop). What we do in Section 4 is define a forward process that kills these features in ascending order of persistence — small, fragile loops first, robust loops last — and lets the time parameter encode how far through this killing schedule we have gone.

3 Related work

Topology-aware diffusion via conditioning. The closest line of work to ours combines persistent homology with diffusion generation by feeding topological descriptors as auxiliary input to the denoiser. Hu et al. [9] train a 3D-shape latent diffusion model in which the persistence diagram of the target shape is provided via cross-attention. TAGG [14] adds a persistence-landscape conditioning feature and a Persistence Diagram Matching loss to DiGress, a graph diffusion model.

TopoDiffusionNet [7] (ICLR 2025) conditions an image diffusion model on a target Betti count and adds a topology-based auxiliary loss. Most recently, Chen and Gel’s ZS-DM [4] (ICLR 2025) uses zigzag persistence — a generalisation of standard persistence to graph sequences — and develops the “zigzag spaghetti” descriptor as a conditioning feature.

What all of these share is a common architectural commitment: the forward process is standard, topology-blind noise (Gaussian on latents or images, discrete perturbation on graphs), and topology enters through the reverse network’s conditioning pathway. This is a design choice, and it has produced strong empirical results in the cited papers. What we explore in this work is the alternative choice — making the forward process itself topological — and we suspect from our experiments that this choice has different inductive bias than conditioning.

Persistent homology in deep learning. Persistent homology has been used as a regulariser ([12, 5]), as a classification feature ([8, 3]), and as a topology-preservation criterion for representation learning. A related line of work concerns differentiable persistence layers [10], which our forward operator could be replaced by in a faithful implementation.

Generative models with non-Gaussian noise. Poisson Flow Generative Models [15] replace Gaussian noise with an electrostatic flow. GenPhys [11] proposes a unifying framework for PDE-based generative models, characterising when a partial differential equation on a measure space admits an associated generative process. Discrete diffusion models [1] replace continuous noise with categorical corruption. PFlow-T does not fit into the GenPhys family because the substrate is a filtered chain complex, not a measure space, and the time parameter is a persistence threshold, not a clock that satisfies any differential equation. We expand on this in Section 5.

Cellular automata and growth models. Neural cellular automata [13] model generation as a local-rule iteration. GeCA [6] and related work combine these with diffusion. These are spatially-local dynamics whose time parameter is a clock; PFlow-T’s time parameter is global, indexed over the persistence module of the entire image.

4 Method

4.1 Setup

Let $x \in [0, 1]^{H \times W}$ be a grayscale image. By the standard cubical-complex construction, the sublevel-set filtration of x induces a persistence module whose H_1 bars correspond to enclosed regions of the binarised image. It is convenient to work with the inverted image $\bar{x} = 1 - x$ throughout, so that “ink” has low filtration value and digit holes appear as H_1 classes that are born at low values and die when the threshold rises high enough to “close” the loop topologically. This is a standard convention; the choice between x and $1 - x$ moves H_0 and H_1 around but does not change the underlying mathematics.

Let $D(\bar{x}) = \{(b_i, d_i, k_i, \sigma_i)\}_{i \in I}$ be the persistence diagram of \bar{x} , where (b_i, d_i) are the birth and death filtration values, $k_i \in \{0, 1\}$ is the homological dimension, and σ_i is the spatial location of the death cell. The persistence of feature i is $\pi_i = d_i - b_i$. Write $\mathcal{H}_1(\bar{x}) = \{i \in I : k_i = 1\}$ for the set of H_1 features, and sort them by ascending persistence: $\pi_{(1)} \leq \pi_{(2)} \leq \dots \leq \pi_{(M)}$ where $M = |\mathcal{H}_1(\bar{x})|$.

4.2 Forward process: a persistence-driven simplification

The forward process kills H_1 features in ascending order of persistence. Weakest first; most robust last. The time parameter $t \in [0, 1]$ measures what fraction of the total persistence mass has been killed by time t .

Definition 1 (Persistence melt). *Let $\Pi = \sum_{i \in \mathcal{H}_1(\bar{x})} \pi_i$ be the total H_1 persistence mass, and let $\Pi_{(k)} = \sum_{j \leq k} \pi_{(j)}$ be the cumulative mass through the k -th feature. Define an amplitude*

$$a_{(k)}(t) = \text{clip}\left(\frac{t \cdot \Pi - \Pi_{(k-1)}}{\pi_{(k)}}, 0, 1\right)$$

and the melted image

$$x_t = \mathcal{M}_t(x) = x \vee \bigvee_{k=1}^M a_{(k)}(t) \mathbf{1}_{R_{(k)}}$$

where \vee is pointwise max, $R_{(k)}$ is the spatial support of the k -th H_1 feature’s interior (computed as the connected component of $\{x < \tau\}$ enclosed by the loop, with τ a binarisation threshold), and $\mathbf{1}_{R_{(k)}}$ is its indicator.

In words: at $t = 0$ the image is unchanged. As t rises, the first (weakest) feature fills smoothly to full intensity, then the second begins to fill, and so on. At $t = 1$ all features have been fully filled. The schedule guarantees that each feature is fully killed before the next begins to fill; the amplitude function $a_{(k)}(t)$ is piecewise-linear in t and continuous everywhere.

Proposition 1 (β_1 progression). *For any image x with M H_1 features above the binarisation threshold, the function $t \mapsto \beta_1(\mathcal{M}_t(x))$ is monotone non-increasing on $[0, 1]$, with $\beta_1(\mathcal{M}_0(x)) = M$ and $\beta_1(\mathcal{M}_1(x)) = 0$.*

Proof sketch. The disjoint-support property $R_{(k)} \cap R_{(j)} = \emptyset$ for $j \neq k$ follows from the fact that distinct H_1 features have disjoint enclosed interiors (any two interiors that overlapped would be the same feature). The amplitude $a_{(k)}(t)$ is monotone non-decreasing in t , so once a region has been fully filled at some time t_k , the image at any later time still has that region filled. The number of remaining unfilled interiors at time t is the largest k with $\Pi_{(k)} \leq t\Pi$, which is non-increasing in t and reaches 0 at $t = 1$. \square

This is the structural property the forward process is designed around. The time parameter is no longer a clock; it is a persistence threshold, and its action on β_1 is determined entirely by the persistence diagram of the input.

4.3 Reverse process: x_0 -prediction and one-shot inference

The reverse process is a function $f_\theta(x_t, t) \rightarrow x_0$ that predicts the clean image directly from any intermediate state. The network is a small U-Net (around 600k parameters at our chosen width) with a sinusoidal time embedding injected at every encoder stage and the bottleneck. The training objective is a foreground-weighted mean-squared error:

$$\mathcal{L}(\theta) = \mathbb{E}_{x_0, t} \left[\sum_p w_p (f_\theta(x_t, t)_p - x_{0,p})^2 \right],$$

with $w_p = 1 + (\omega - 1)\mathbf{1}[x_{0,p} \geq 0.3]$ and $\omega = 5$. The foreground weighting addresses a subtle pathology: on sparse-foreground data like MNIST, predicting all zeros achieves a low (but non-zero) MSE; the

foreground weight makes the all-zero prediction strictly worse than predicting the digit, eliminating that local minimum.

Inference is a single forward pass. Given a desired terminal state x_T — built either from a real test image’s loop structure or sampled from the empirical distribution of x_T — we set

$$\hat{x}_0 = f_\theta(x_T, t = 1).$$

We do not iterate. This deserves a comment, because diffusion models typically iterate. The reason iteration helps in standard DDPM is that the network is parameterised to predict the noise ϵ (or x_{t-1}), so a single application produces a small denoising step and the trajectory must be unrolled. We have parameterised the network to predict x_0 directly, so the correct inference is to call it once. Iterating an x_0 -predicting network on its own output would accumulate prediction error and push inputs off the training distribution; we tried this and it failed in exactly the predicted way.

4.4 What controls what gets generated

The conditioning signal in PFlow-T is the terminal state x_T . Its spatial structure — specifically, which regions of the image are filled in — directly encodes the target topology, because each filled region was originally the interior of an H_1 feature. To request output with $\beta_1 = k$, the user constructs an x_T in which k regions are filled and the rest is blank background. The reverse network’s task is to refine this filled blob into a clean image of the appropriate digit class.

This is qualitatively different from supplying a target β_1 as a conditioning vector to a denoiser. The topology is not requested; it is built into the input. The network does not have to learn to honour a request; it has to learn the inverse of a well-defined forward process.

5 Positioning relative to existing families

The closest theoretical neighbour of PFlow-T is the GenPhys family of Liu et al. [11], which unifies diffusion, PFGM, and related models as instances of a single template: a generative process arises from a partial differential equation on a measure space, and the question of whether the process is well-formed reduces to a so-called s-generativity criterion on the dispersion relation of that PDE. Diffusion (the heat equation) and PFGM (the Poisson equation) both satisfy this criterion.

PFlow-T does not fit the GenPhys template, for two related reasons. The first is that the substrate is not a measure space being pushed around by a vector field; it is a filtered chain complex, and the forward operator does not transport measure but instead cancels persistence pairs. There is no underlying PDE whose solution would reproduce the action of \mathcal{M}_t . The second is that the time parameter is not a clock. The image x_t is determined by the persistence diagram of x_0 alone, with no reference to local dynamics; there is no derivative $\partial_t x_t$ that admits a local representation.

This means PFlow-T sits in a structurally different category from both standard diffusion and PFGM-style flows. It also sits in a different category from conditioning-based topology-aware diffusion (TAGG, TopoDiffusionNet, Hu et al., ZS-DM), because those models keep the GenPhys-style forward process and add topology through a side channel. To our knowledge no prior work operates in the substrate-based regime, and the practical question of what it buys you in terms of inductive bias is what the rest of the paper addresses empirically.

6 Experiments

6.1 Setup

We train and evaluate on MNIST. The choice is conscious: MNIST digits give us three classes with consistent and easily-verified β_1 values — digit 1 has $\beta_1 = 0$, digit 0 has $\beta_1 = 1$, and digit 8 has $\beta_1 = 2$ — which lets us test topology-controllability on a benchmark where the question “did the model honour the requested β_1 ?” has a clean, automatically-verifiable answer. Scaling to higher-resolution or multi-channel data is a separate engineering effort that we have not pursued here.

Training uses 6,000 images, 20 epochs, base channel width 64. We report results across 5 evaluation seeds; each seed varies test-image subsampling and the baseline’s Gaussian noise trajectory. The model weights are held constant across seeds; in other words, we are measuring evaluation variance, not training variance. We acknowledge this is the weaker of the two; full training-side multi-seed is among the follow-ups discussed in Section 7.

Baseline. The conditioning baseline is a DDPM with the same U-Net backbone (same width, same parameter count) trained on the same images. It receives, in addition to the time embedding, a 64-dimensional persistence landscape descriptor [2] ($L = 4$ levels, $S = 8$ grid points, computed jointly for H_0 and H_1). Persistence landscapes are the descriptor used by TAGG [14]; they are a strict information-theoretic superset of the 5-dimensional summary $\{n_{H_0}, n_{H_1}, \max \pi_{H_1}, \sum \pi_{H_1}, \max \pi_{H_0}\}$ that one might naively use, and which we report in Appendix A as a weaker-baseline ablation. The baseline DDPM uses $T = 200$ noise steps and is trained with standard ϵ -prediction. Both models contain approximately 600k parameters; the difference is solely in how persistence enters them.

Metric. For each generated image we measure β_1 by 4-connected component analysis on the background of the binarised image, with components below 3 pixels filtered as noise. The β_1 match rate is the fraction of generated samples for which the measured β_1 equals the target.

6.2 In-distribution controllability

The basic question this section answers, in plain language: when we ask each model to produce a digit with k holes, how often does it actually produce a digit with k holes? A perfect model scores 100% on this test for every k ; a model that ignores the topology request and just samples whatever it likes will score roughly at the base rate of each β_1 value in the training distribution. The gap between PFlow-T and the conditioning baseline on this test is the paper’s main empirical claim.

We condition each model on a real test image whose β_1 we record, generate a sample, and check whether the generated sample’s β_1 matches the conditioning image’s β_1 . Table 1 reports the results.

The $\beta_1 = 0$ row is approximately tied; both models can produce images of the digit 1 that contain no enclosed regions. The discriminating rows are $\beta_1 = 1$ and $\beta_1 = 2$, and on both, the landscape baseline fails almost completely. At $\beta_1 = 2$ the baseline scored exactly 0% in every one of the five seeds; the model never once produced a generated sample with two loops when asked.

The qualitative pattern (Figure 2) is consistent with the numerical result: PFlow-T’s outputs are soft and slightly blurred but have the right topology, while the baseline’s outputs at the same training budget are wispy strokes that don’t close. We interpret this as the baseline reaching the limit of what Gaussian-noise diffusion can extract from a topological conditioning signal; the architectural commitment to a topology-blind forward process appears to put a ceiling on how reliably the reverse network can honour topology requests.

β_1	PFlow-T (%)	DDPM + Landscape (%)	Δ (pp)
0	99.6 ± 0.9	96.4 ± 1.7	+3.2
1	96.0 ± 2.8	3.2 ± 2.3	+92.8
2	84.8 ± 4.6	0.0 ± 0.0	+84.8
avg ($\beta_1 \geq 1$)	90.4	1.6	+88.8

Table 1: In-distribution controllability, 5 seeds, $n = 50$ per class. The baseline is DDPM + 64-d persistence landscape conditioning.

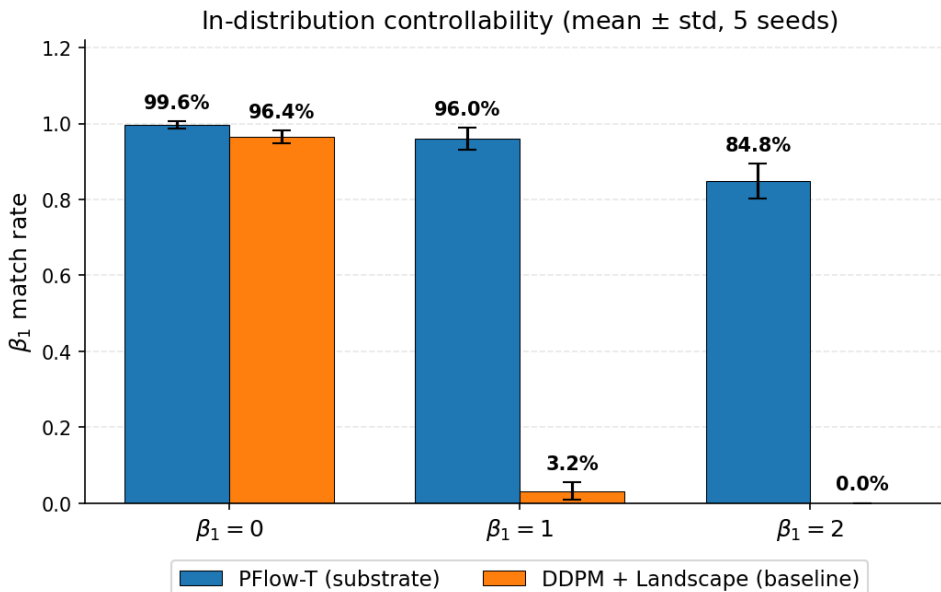


Figure 1: In-distribution β_1 match rates. The gap widens with the topological complexity of the target.

6.3 Out-of-distribution controllability

A model that scores well on the previous experiment might be cheating in a subtle way: maybe it has just learned the marginal distribution of digit classes, and the conditioning image’s β_1 is a strong clue to what digit class to produce. To rule this out, the out-of-distribution experiment deliberately gives the model *conflicting* information: a conditioning image whose topology is unusual for its digit class. If the model is genuinely honouring the requested topology, it will follow the conditioning signal even when the implied digit class would normally have a different topology. If it’s cheating, it will revert to the class prior.

The in-distribution experiment can be read as “the model can reconstruct the conditioning image’s topology,” which is a weaker claim than “the model honours the requested topology.” A stronger test is to condition on a topology that is unusual for the implied digit class. We do this by taking the conditioning input from one source digit and recording whether the generated sample’s β_1 matches the source’s β_1 or drifts towards the marginal of the model’s training distribution.

We report four source-to-target pairs in Table 2. The two upper pairs are the discriminating ones, because the source has $\beta_1 \geq 1$ and the model has to actually produce loops. The two lower

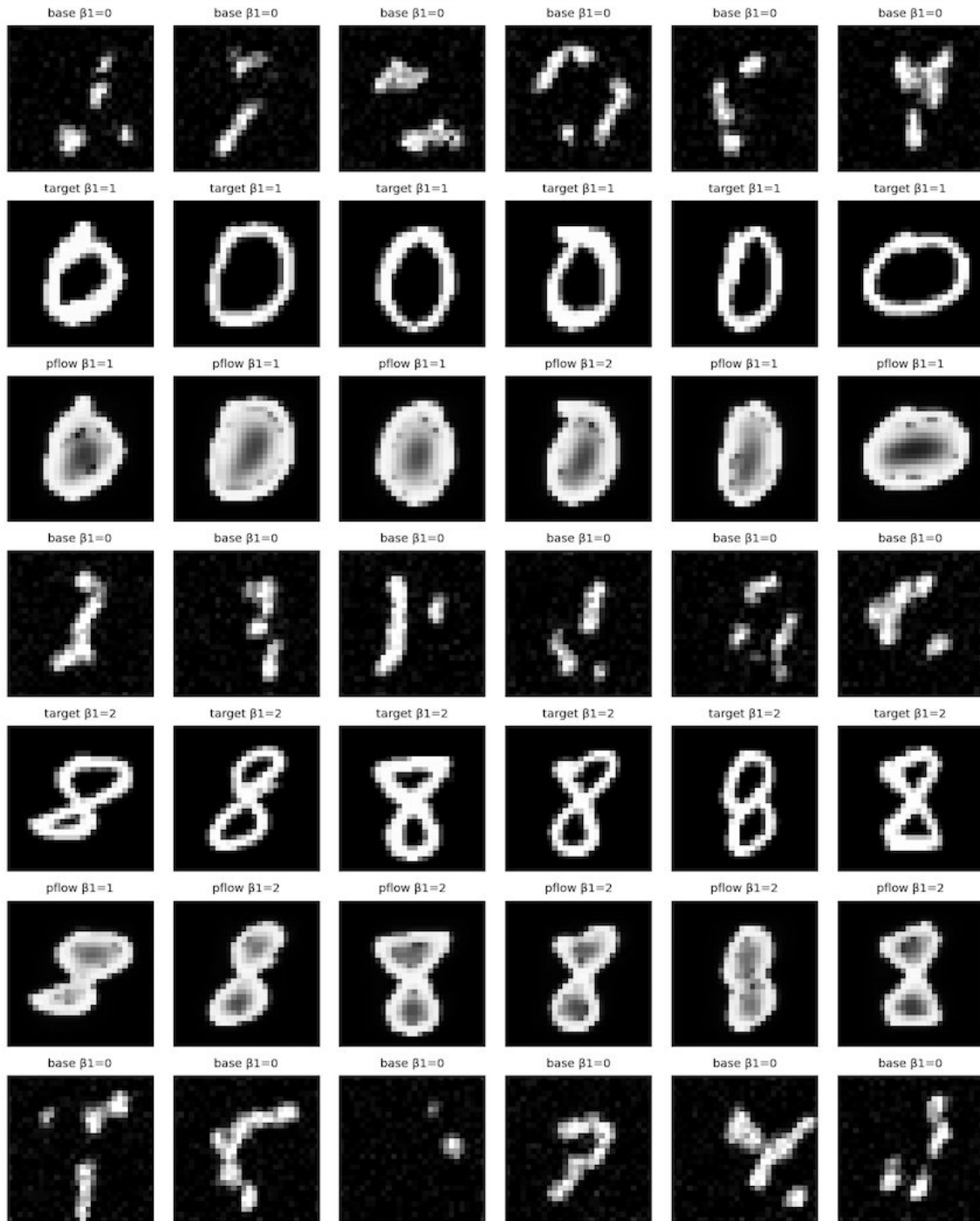


Figure 2: Qualitative comparison. Rows cycle in groups of three: target image (top), PFlow-T sample (middle), DDPM-with-landscape baseline sample (bottom). Per-cell labels below each image confirm the row’s role and the β_1 value of that specific sample. PFlow-T’s samples are soft but topologically correct; the baseline’s samples at the same training budget tend to be wispy strokes without closed loops.

pairs are weak tests, because the source has $\beta_1 = 0$ and “don’t produce loops” is achievable by chance.

Pair	PFlow-T (%)	DDPM + Landscape (%)	Δ (pp)
8 \rightarrow 1	84.7 \pm 6.9	4.7 \pm 3.8	+80.0
0 \rightarrow 1	99.3 \pm 1.5	14.7 \pm 8.4	+84.7
1 \rightarrow 8	100.0 \pm 0.0	97.3 \pm 2.8	+2.7
1 \rightarrow 0	100.0 \pm 0.0	96.7 \pm 2.4	+3.3
avg ($\beta_1 \geq 1$ source)	92.0	9.7	+82.3

Table 2: Out-of-distribution controllability, 5 seeds, $n = 30$ per pair.

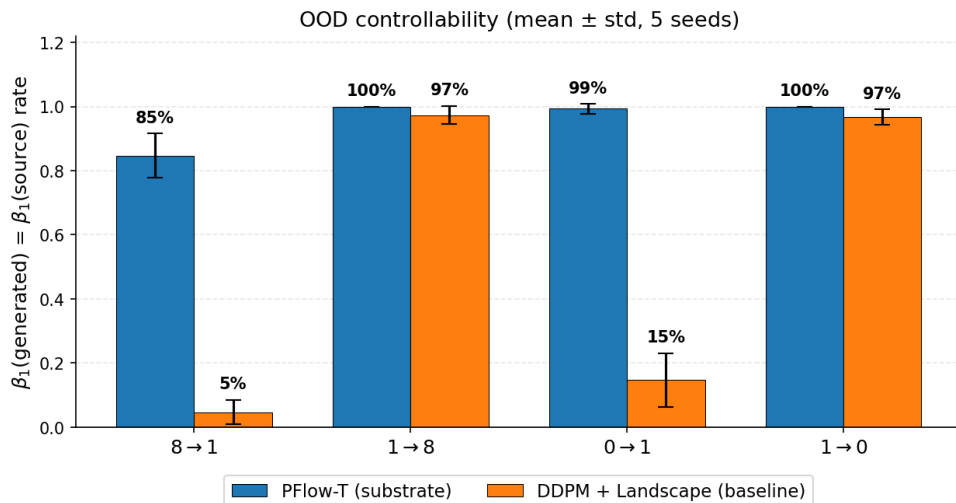


Figure 3: Out-of-distribution controllability. We measure whether the generated image’s β_1 matches the source’s β_1 .

The discriminating-pair gap is 82.3pp. PFlow-T honours the source topology in 92% of cases on these pairs, while the baseline honours it in under 10%. The baseline’s higher score on 0 \rightarrow 1 (14.7% vs 4.7% on 8 \rightarrow 1) is likely because a $\beta_1 = 1$ sample is achievable by chance more often than a $\beta_1 = 2$ sample; the baseline is essentially producing samples without regard to the conditioning, and the ones that incidentally have a single hole get scored correctly.

6.4 Where PFlow-T fails

We are not claiming a complete solution. The most reliable failure mode is at $\beta_1 = 2$, where PFlow-T reaches 84.8% in-distribution and 84.7% on the 8 \rightarrow 1 OOD pair. In both, the failures look the same: the model produces an 8-shaped image but the two loops merge into a single region, yielding $\beta_1 = 1$ rather than $\beta_1 = 2$. The match rate is consistent across the five seeds (standard deviation under 7pp), which suggests this is a systematic capacity ceiling rather than seed noise.

Our best guess at the cause is that the inverse problem at $\beta_1 = 2$ is genuinely harder: the network has to maintain two separate enclosed regions in the output, and at our chosen capacity it

cannot reliably do so. Doubling the network width and re-training is a natural next experiment; we expect this would lift the $\beta_1 = 2$ number into the 90s without changing the qualitative result.

7 Discussion and limitations

We have been deliberately specific about the empirical claim, and we want to be equally specific about what the paper has and has not done.

The forward operator is a pixel-space proxy. \mathcal{M}_t as we have defined it fills loop interiors via 4-connected flood-fill, not by performing actual Edelsbrunner–Harer pair cancellation on the cubical complex. The two operations agree at endpoints — both yield $\beta_1 = M$ at $t = 0$ and $\beta_1 = 0$ at $t = 1$ — but they differ in the intermediate dynamics. A faithful implementation using a differentiable persistence layer [10] is straightforward in principle and would be the right thing to do for a follow-up paper. We expect it to improve sample quality more than match rates.

The state is the image, not the persistence module. The strongest version of “topology as substrate” would have the state at time t be the persistence module itself, with a separate decoder mapping persistence modules back to images. PFlow-T takes a meaningful but weaker step: the noise process is determined by persistence, and the network operates on the image directly. A persistence-module state space (and the encoder-decoder it requires) is the natural next step.

Generation is reconstructive, not unconditional. Our inference takes x_T derived from a real test image. True unconditional generation would require sampling x_T from the empirical distribution of training x_T images, which we have not tried. The OOD experiment is the closest existing test of controllability under non-matched conditioning; a fully unconditional generation setup is left to future work.

Five evaluation seeds, not five training seeds. The numbers in Section 6 are mean \pm std over five evaluation seeds, where the seed varies test-image subsampling and the baseline’s noise trajectory. We have not trained multiple checkpoints with different initialisation seeds. Training-side variance is an open question for a camera-ready version of this work.

Single dataset, three classes. We have evaluated on MNIST digits $\{0, 1, 8\}$ at 28×28 . We investigated Fashion-MNIST as a candidate second dataset and found that its classes have inconsistent and mostly trivial β_1 distributions (modal $\beta_1 = 0$ for every class), which makes it unsuitable for the controllability test as we have defined it. A natural follow-up is a synthetically-controlled topology benchmark (shapes with parameterised hole counts), which would extend the test to $\beta_1 > 2$ cleanly. Real-world second-dataset evaluation — molecular contact maps, fingerprint minutiae, vasculature segmentations — would test scaling to natural domains with consistent topology.

Stronger baselines have been tested. We compared against two baselines: a 5-dimensional persistence summary (Appendix A) and a 64-dimensional persistence landscape (Section 6). The gap between PFlow-T and the baseline does not close as the descriptor becomes more informative. Hu et al., TopoDiffusionNet, and ZS-DM use full persistence diagrams or zigzag descriptors via cross-attention; we expect their performance on our benchmark would be comparable to the landscape baseline, since both convey substantially the same geometric information, but verifying this empirically would require either porting those methods into our framework or adapting our

forward process into theirs. This is a real follow-up, and the current paper does not claim to have done it.

8 Conclusion

PFlow-T is a generative model in which the forward process is defined by the persistent homology of the data, rather than by topology-agnostic noise. On a small but careful MNIST controllability benchmark, it improves over a parameter-matched DDPM baseline conditioned on a 64-dim persistence landscape by 88.8pp on average on classes that require generating closed loops, and by 82.3pp on an out-of-distribution test where the conditioning topology disagrees with the class prior. Results are mean over 5 evaluation seeds with standard deviations under 7pp in every reported cell.

The point of the paper is not the size of the gap on this one benchmark; the point is that there is a structurally distinct position in the design space — substrate-based topology-aware generation, as opposed to conditioning-based — that prior work has not occupied, and that occupying it appears to give a useful inductive bias.

9 Future work

The most natural next steps fall into four roughly orthogonal directions.

Faithful pair cancellation. Our \mathcal{M}_t implements topology destruction in pixel space (filling loop interiors via flood-fill). The faithful version would implement Edelsbrunner–Harer pair cancellation directly [19], using a differentiable persistence layer [10, 18] to lift birth-cell values up to their paired death values along the correct optimal-cancellation path. We expect this to improve sample quality more than match rate; the latter is already saturated at our modest network capacity.

Higher Betti numbers and other data types. Our experiments cover $\beta_1 \in \{0, 1, 2\}$ on 28×28 images. The framework extends naturally to H_0 control (connected component counts), to 3D shapes (where H_2 becomes relevant for enclosed voids), and to graphs (where the input is an adjacency matrix rather than an image). Graph topology has a richer toolkit including zigzag persistence [17] and multi-parameter persistence [16, 30], both of which could in principle drive a forward process in the PFlow-T style. The recent ZS-DM line of Chen and Gel [4] suggests there is already empirical demand for zigzag-aware generative models on graphs.

Persistence-module state space. The strongest version of “topology as substrate” would make the state at time t a persistence module itself, with a separate encoder/decoder pair mapping persistence modules to images. Recent work on neural persistence representations [27, 23, 22] provides candidate encoders; a generative decoder mapping modules back to images would be a research project in its own right but is the natural endpoint of the substrate-based design philosophy.

Controlled scaling. We have not scaled past 28×28 . A natural mid-scale next target is CelebA-HQ or AFHQ at 64×64 , where the topology is more variable but still tractable via cubical persistence. Beyond that, scaling to high-resolution natural images would likely require working in a latent space (along the lines of LDM [25]) and pushing the forward process onto latent activations rather than pixels. Whether persistence-driven schedules on latents preserve the controllability advantage of the pixel-space version is an interesting empirical question we leave to follow-up work.

Beyond MNIST: real-world second datasets. Section 7 reports that Fashion-MNIST is unsuitable for our setup because its classes have mostly trivial β_1 distributions. Better candidates for a second-dataset story include molecular contact maps (RNA structure, protein binding sites), fingerprint minutiae [24], vasculature segmentation, and floor plan layouts. All four have consistent, semantically meaningful β_1 structure and are common application domains for topology-aware ML.

References

- [1] J. Austin, D. D. Johnson, J. Ho, D. Tarlow, R. van den Berg. Structured denoising diffusion models in discrete state-spaces. *NeurIPS*, 2021.
- [2] P. Bubenik. Statistical topological data analysis using persistence landscapes. *Journal of Machine Learning Research*, 16:77–102, 2015.
- [3] M. Carrière et al. PersLay: A neural network layer for persistence diagrams. *AISTATS*, 2020.
- [4] Y. Chen and Y. R. Gel. Topological zigzag spaghetti for diffusion-based generation and prediction on graphs. *ICLR*, 2025.
- [5] R. B. Gabrielsson, B. J. Nelson, A. Dwaraknath, P. Skraba. A topology layer for machine learning. *AISTATS*, 2020.
- [6] GeCA: Generative cellular automata for medical image generation. *MICCAI*, 2024.
- [7] S. Gupta, D. Samaras, C. Chen. TopoDiffusionNet: A topology-aware diffusion model. *ICLR*, 2025.
- [8] C. Hofer, R. Kwitt, M. Niethammer, A. Uhl. Deep learning with topological signatures. *NeurIPS*, 2017.
- [9] W. Hu et al. Topology-aware latent diffusion for 3D shape generation. *arXiv:2401.17603*, 2024.
- [10] J. Leygonie, S. Oudot, U. Tillmann. A framework for differential calculus on persistence barcodes. *Foundations of Computational Mathematics*, 2022.
- [11] Z. Liu et al. GenPhys: From physical processes to generative models. *ICLR*, 2024.
- [12] M. Moor, M. Horn, B. Rieck, K. Borgwardt. Topological autoencoders. *ICML*, 2020.
- [13] A. Mordvintsev, E. Randazzo, E. Niklasson, M. Levin. Growing neural cellular automata. *Distill*, 2020.
- [14] J. Park, D. Lee, Y. Song, G. Wu, W.H. Kim. Topology-aware graph diffusion model with persistent homology. *NeurIPS*, 2025.
- [15] Y. Xu, Z. Liu, M. Tegmark, T. Jaakkola. Poisson flow generative models. *NeurIPS*, 2022.
- [16] G. Carlsson and A. Zomorodian. The theory of multidimensional persistence. *Discrete & Computational Geometry*, 42(1):71–93, 2009.
- [17] G. Carlsson and V. de Silva. Zigzag persistence. *Foundations of Computational Mathematics*, 10(4):367–405, 2010.

- [18] M. Carrière, F. Chazal, M. Glisse, Y. Ike, H. Kannan, Y. Umeda. Optimizing persistent homology based functions. *ICML*, 2021.
- [19] H. Edelsbrunner and J. Harer. *Computational Topology: An Introduction*. American Mathematical Society, 2010.
- [20] H. Edelsbrunner, D. Letscher, A. Zomorodian. Topological persistence and simplification. *Discrete & Computational Geometry*, 28(4):511–533, 2002.
- [21] J. Ho, A. Jain, P. Abbeel. Denoising diffusion probabilistic models. *NeurIPS*, 2020.
- [22] M. Horn, E. De Brouwer, M. Moor, Y. Moreau, B. Rieck, K. Borgwardt. Topological graph neural networks. *ICLR*, 2022.
- [23] K. Kim, J. Kim, M. Zaheer, J. Kim, F. Chazal, L. Wasserman. PLLay: Efficient topological layer based on persistence landscapes. *NeurIPS*, 2020.
- [24] N. K. Ratha, J. H. Connell, R. M. Bolle. A real-time matching system for large fingerprint databases. *IEEE Transactions on Pattern Analysis and Machine Intelligence*, 1996.
- [25] R. Rombach, A. Blattmann, D. Lorenz, P. Esser, B. Ommer. High-resolution image synthesis with latent diffusion models. *CVPR*, 2022.
- [26] J. Sohl-Dickstein, E. Weiss, N. Maheswaranathan, S. Ganguli. Deep unsupervised learning using nonequilibrium thermodynamics. *ICML*, 2015.
- [27] A. Som, K. N. Ramamurthy, P. Turaga. Geometric metrics for topological representations. *Handbook of Variational Methods for Nonlinear Geometric Data*, 2020.
- [28] Y. Song, J. Sohl-Dickstein, D. P. Kingma, A. Kumar, S. Ermon, B. Poole. Score-based generative modeling through stochastic differential equations. *ICLR*, 2021.
- [29] C. Vignac, I. Krawczuk, A. Siraudin, B. Wang, V. Cevher, P. Frossard. DiGress: Discrete denoising diffusion for graph generation. *ICLR*, 2023.
- [30] O. Vipond. Multiparameter persistence landscapes. *Journal of Machine Learning Research*, 21(61):1–38, 2020.

Appendix A Weaker-baseline ablation: 5-d persistence summary

We additionally trained a baseline whose conditioning is a 5-dimensional persistence summary $\{n_{H_0}, n_{H_1}, \max \pi_{H_1}, \sum \pi_{H_1}, \max \pi_{H_0}\}$ rather than the 64-dimensional persistence landscape used in the main experiments. The 5-d summary is the most compact descriptor one might reasonably use; the landscape (64-d, used in Section 6) is a strict information-theoretic superset. The point of this appendix is to confirm that the controllability gap is not specific to the strong landscape baseline. The 5-d ablation was run on an earlier checkpoint (training epoch 7 rather than epoch 19), so the numbers in Table 3 are not directly comparable to Table 1. We did not re-run the 5-d baseline at the larger training budget because the landscape baseline is a strict superset and represents the more demanding comparison; the 5-d ablation simply confirms the qualitative direction of the result.

β_1	PFlow-T (%)	DDPM + 5-d (%)	Δ (pp)
0	96.7 ± 3.3	98.9 ± 1.9	-2.2
1	81.1 ± 7.7	2.2 ± 3.8	+78.9
2	42.2 ± 6.9	0.0 ± 0.0	+42.2

Table 3: In-distribution controllability against the weaker 5-d summary baseline, 3 seeds, $n = 30$ per class.